Solar Physics (2005) 228: 361–375

SOLAR FEATURE CATALOGUES IN EGSO

V. V. ZHARKOVA
Department of Cybernetics, Bradford University, Bradford BD7 1DP, U.K.
(e-mail: v.v.zharkova@brad.ac.uk)

J. ABOUDARHAM
LESIA, The Paris-Meudon Observatory, F92195 Meudon Principal, Cedex, France

S. ZHARKOV, S. S. IPSON and A. K. BENKHALIL
Department of Cybernetics, Bradford University, Bradford BD7 1DP, U.K.

and

N. FULLER
LESIA, The Paris-Meudon Observatory, F92195 Meudon Principal, Cedex, France

(Received 31 January 2005; accepted 25 February 2005)

Abstract. The Solar Feature Catalogues (SFCs) are created from digitized solar images using automated pattern recognition techniques developed in the European Grid of Solar Observation (EGSO) project. The techniques were applied for detection of sunspots, active regions and filaments in the automatically standardized full-disk solar images in CaII K1, CaII K3 and Hα taken at the Meudon Observatory and white-light images and magnetograms from SOHO/MDI. The results of automated recognition are verified with the manual synoptic maps and available statistical data from other observatories that revealed high detection accuracy. A structured database of the Solar Feature Catalogues is built on the MySQL server for every feature from their recognized parameters and cross-referenced to the original observations. The SFCs are published on the Bradford University web site *http://www.cyber.brad.ac.uk/egso/SFC/* with the pre-designed web pages for a search by time, size and location. The SFCs with 9 year coverage (1996–2004) provide any possible information that can be extracted from full disk digital solar images. Thus information can be used for deeper investigation of the feature origin and association with other features for their automated classification and solar activity forecast.

1. Introduction

The automated detection and verification of various features of interest is becoming increasingly important for processing the increased amount of data produced by the current and future space and ground-based instruments. The data volume threatens to overwhelm observers with information to be included into reliable forecasts of solar activity and space weather that require applying a modern level of intelligent data mining taking into account the whole available set with the most recent observations included. This can only be achieved with automation of the procedures of data processing including their standardization to some generic levels, automated extraction of the features of interest from digital images, population into the databases used for the solar models and refinement of these models with respect

to the new data. Inevitably, this raises the accuracy and reliability requirements of the detection techniques applied for an automated recognition that have to be significantly improved in comparison with the existing manual ones.

There is a growing number of archives of digitized images of the Sun, taken from ground-based and space instruments in various wavelengths. These archives are available from different locations and are to be included into a unified catalogue by the European Grid for Solar Observations (EGSO) project (Bentley and EGSO Consortium, 2002). Digitized solar images from different sources have a variety of sizes, resolutions, dynamic ranges and instrumental and weather associated distortions. All are to be subjected to automated recognition processes in order to provide reliable data on the locations of features and their evolution at different times relative to solar rotation. One of the main objectives for EGSO Project Work Package 5 is a production of Solar Feature Catalogues by means of automated feature recognition methods.

This is aimed partly at the growing demand for solar activity forecasts by the space weather project and by many industrial organizations, which have a great need for the development of reliable and fast techniques for feature recognition on solar disks and their presentation in Solar Feature Catalogues. These catalogues are intended to contain comprehensive statistics of active events (sunspots, active regions, filaments, flares, etc.), overlapping in a given period of time and to allow the extraction of physical characteristics, which are essential for solar activity forecasts.

This requires designing advanced image recognition techniques in order to identify individual features (sunspots, active regions, filaments, magnetic neutral lines, etc.) on the images with strongly varying background caused by different terrestrial atmosphere observing conditions of solar atmosphere activity period, irregularities in shape caused by instrumental errors or any other noise in images like strips or signatures etc. For added reliability, these algorithms have to use cross-referenced criteria at multiple wavelengths in order to correctly identify the features of interest while fully utilizing all the datasets linked into the Grid.

The following sections describe some of the feature recognition techniques summarized in a review (Zharkov, Zharkova, and Ipson, 2005). The techniques for image pre-processing are briefly described in Section 2 and for the automated detection of the selected solar features: sunspots, active regions and filaments including their magnetic fields in Section 3. Also in Section 4 we present a scheme of the relational database in which these data are populated and linked with data queries via the EGSO web broker.

2. Automated Image Standardization Technique

There are a number of difficulties that can occur with a solar image as is demonstrated in Figure 1: errors in FITS header information; image shape (ellipse), error in the centre and the pole coordinates; weather transparency (clouds) and

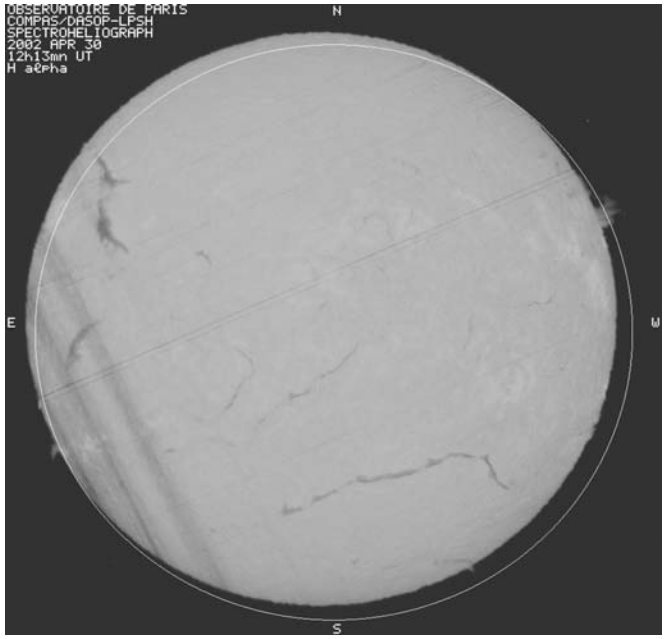

Figure 1. A sample solar image demonstrates the distortions in intensity (strips, limb darkening) and elliptical shape. The white-line circle shows the solar disk position taken from the image header.

different thickness of atmosphere; center-to-limb darkening; defects in data (strips, lines, intensity). These original observation data with the header are stored in an *observation table* of the SFC database (see Section 4).

When the geometrical information provided in image headers is not correct and the external photometric effects are to be removed this requires automated procedures to be developed. These geometric and intensity effects are checked with robust techniques developed for full disk solar images in order to convert them into a standardized form of a 'virtual solar image', or a flat image, free of geometrical distortions and limb darkening (Zharkova *et al.*, 2003). The technique was applied for Hα and Ca K lines full-disk images taken at the Meudon Observatory and for the SOHO/MDI white-light images. This provided a fully standardized approach to the features detected in any images from these archives; although, the technique adjustment based on the nature of distortion is required for any other archives produced by different instruments.

The limb fitting starts with an initial estimate of the solar centre using raw 12-bit image data and then applies a Canny edge-detection routine (Canny, 1986). Candidate edge points for the limb are selected using a histogram based method and the chosen points fitted to a quadratic function by minimizing the algebraic distance using Singular Value Decomposition (SVD) (Baxes, 1994). The five parameters of the ellipse fitting the limb are extracted from the quadratic function. These

parameters are used to define an affine transformation that transforms the image shape into a circle. Transformed images are generated using the nearest neighbor, bilinear or bicubic interpolation. Intensity renormalization is also required because of a limb darkening and other non-radial intensity variations. It is achieved by fitting a background function in polar co-ordinates to a set of sample points having the median intensities (Casasent, 1992) and by standardizing the average brightness (for more details about the standardization technique see Zharkova *et al.*, 2003).

The parameters used for an image preprocessing, or standardization, including a code version and procedures applied are stored in a *pre-processing table* of the SFC database (see Section 4).

3. Automated Feature Recognition Techniques

3.1. SUNSPOT DETECTION

The sunspots are darker features with strong magnetic field occurring in the solar photosphere on a "quiet Sun" background that can be observed in both SOHO/MDI white light and CaII K1 spectral line images. Visually, they consist of the two parts: a dark, roughly circular central disk called the umbra, and a lighter outer area called the penumbra. Sunspots are most clearly observed in the "white light" images, but the stronger spots can be also detected in the CaII K1 images due to their strong absorption.

Sunspot identification is required for a quantitative study of the solar cycle and this includes determining their locations, lifetimes, contrasts and other characteristics. Sunspot identification also plays an essential part in modeling of the total solar irradiance (TSI) and the variations of sunspot properties with latitude and phase in the solar cycle. Sunspots are also part of solar active regions, and their local behavior is used in the study of active region evolution and for a forecast of the solar activity.

Early thresholding methods of sunspot detection in digital full solar images (Chapman and Groisman, 1984; Steinegger *et al.*, 1990; Brandt, Schmidt, and Steinegger, 1990) were refined by using image histograms to determine the threshold levels (Chapman, Cookson, and Dobias, 1994; Steinegger *et al*., 1996, 1997). An automated approach to sunspot detection includes the Bayesian technique developed for active region and sunspot detection (Turmon, Pap, and Mukhtar, 2002) that is more oriented towards faculae detection and does not detect sunspot umbrae. The semi-automated method, based on region growing technique by utilizing sunspot contrast and contiguity was developed for full disk solar images (Preminger, Walton, and Chapman, 2001). A more precise automated approach to sunspot area measurements with edge detection and boundary gradient intensity was suggested for high-resolution observations of individual sunspot groups (Györi, 1998). The method is very accurate when applied to data with sufficiently high resolution but

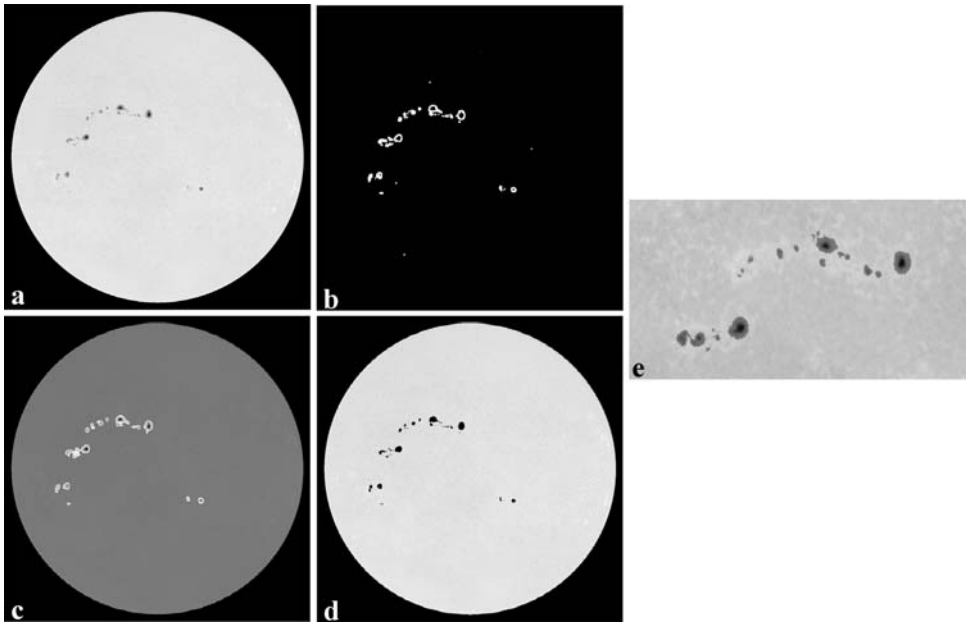

Figure 2. Sunspot detection performed on a CaII K1 line full-disk image obtained from the Meudon Observatory. (a) The original image after cleaning; (b) the final detection results superimposed on original image; (c) image after a watershed operator is applied; (d) and (e) close-up of detected umbrae and penumbras in (b) (from Zharkov *et al.*, 2005b).

in its original form is not suitable for the automatic detection and identification of sunspots on full-disk images.

The technique for sunspot detection developed as a part of Work Package 5 (Zharkov *et al.*, 2003, 2004; Zharkov, Zharkova, and Ipson, 2005) is fully automated and includes the advantages of the methods described above. The sample results of the application of this automated technique on the SOHO/MDI white-light full-disk images are presented in Figure 2. The process involves pre-processing of the full disk high-resolution solar image (Figure 2a) by correcting, if necessary, the shape of the disk to a circular one and by removing limb-darkening as described in Section 2 (Zharkova *et al.*, 2003). Then a morphological gradient operator is applied to edge enhance the image (Baxes, 1994), followed by thresholding in order to detect only strong edges (Figure 2b). After removing the limb edge, a watershed operator is applied to the binary image in order to fill the sunspot area enclosed by the edges (Jackway, 1996). Further median filtering is used (Casasent, 1992) to eliminate noise and smaller features (Figure 2c). The regions' statistical properties are then used for the removal of false identifications such as, for example, the artifacts and lines, often present in the Meudon Observatory images. For the extraction of the area, shape, umbra/penumbra location of the detected sunspots and their basic classification the Canny edge detection technique (Canny, 1986) is

used and with the detection results presented in Figure 2d (full disk) and Figure 2e (close-up fragment).

The automated sunspot detection technique was tested on two months of daily observations (April and July 2002) of CaII K1 line images and SOHO/MDI white-light images that revealed a good correlation with the manual synoptic maps. A comparison between the automated and manual detections in the Meudon CaII K1 images was done by calculating daily the False Acceptance Rate (FAR) (a feature detected automatically but not manually) and the False Rejection Rate (FRR) (a feature detected manually but not with our technique) for available observations. A Classifier Setting (CS) is accepted to be equal to 1 that corresponds to a total number of Sunspot Candidates detected and CS equal to 5 that represents a number of Sunspot Candidates of sizes with the principal component coefficient less than 2.1 and the mean absolute deviation measured the quiet-Sun intensity is greater than 21. As can be expected, the FFR is lowest for the classifier value of 1 that does not exceed 15.2% from a total sunspot number detected on a day. On the contrary, FAR is lowest for the value of 5 and does not exceed 8.8% from the same number of sunspots.

Hence, one can conclude that the technique applied to sunspot detection on the Meudon CaII K1 full-disk images performs very well in comparison with other earlier methods for full-disk images (see a review in Zharkov, Zharkova, and Ipson, 2005). The technique was then applied to the SOHO/MDI white-light images for the whole period (1996 – 2004) of observations with the detection results including sunspot location, size, number of umbras and intensity range (max and min). The detected sunspot areas were compared with the average sunspot numbers from Sunspot Index Data Center (SIDC), which confirmed a very high (0.86) correlation coefficient between these two sets despite their principal differences (area-numbers) (Zharkov and Zharkova, 2005). A comparison of the temporal variations of daily sunspot areas extracted from the Solar Feature Catalogue with those available from the digitized sunspot drawings at NOAA revealed the highest correlation coefficient of 96% (Zharkov, Zharkova, and Ipson, 2005). In addition, sunspots, detected with the excellent accuracy were overlaid with the SOHO/MDI magnetograms that provided magnetic flux confined in penumbras and umbras with their some statistical properties reported by Zharkov and Zharkova (2005).

The sunspot parameters above are extracted from the SOHO/MDI data obtained in 1996 – 2004 and populated into a *sunspot feature table* of the SFC database, discussed in Section 4.

3.2. ACTIVE-REGION DETECTION

Active regions are the basic reference features for the solar activity. Their reliable automated detection will enable the building of a major database of solar active features and for the first time allow analysis of solar activity on a comprehensive database of active regions taken in various wavelengths.

There are three different approaches identified in the literature for the identification of bright active regions (plages): intensity thresholding (Worden, White, and Woods, 1996; Steinegger and Brandt, 1998; Preminger, Walton, and Chapman, 2001), region growing (Hill *et al.*, 2001; Veronig *et al.*, 2001) and the Bayesian inference method (Turmon, Pap, and Mukhtar, 2002). All these approaches can give a reasonable accuracy of detection with suitable images, while the intensity threshold-based methods are simple and fast, but are relatively sensitive to noise which affects the reliability of the segmentation results obtained and the Bayesian based methods are the most computationally expensive.

The procedures developed in EGSO uses the combination of statistically derived local intensity threshold, morphological filtering, and region growing methods. Techniques are developed for the automated detection of active regions (plages) in solar images obtained from the Meudon Observatory, using the Hα and CaII K3 spectral lines (Benkhalil *et al.*, 2003, 2005) or including EIT images (Benkhalil *et al.*, 2004), aiming to replace the existing manual detection methods (Mouradian, 1998).

The automated technique starts with an initial segmentation of active regions, which is achieved using intensity thresholds determined using statistical information obtained for each quarter of a full-disk solar image. Median filtering (Casasent, 1992) and morphological operations (Baxes, 1994; Jackway, 1996) are applied to the resulting binary image to remove noise and to merge broken regions. Seed pixels selected in each of the initially segmented located regions are used to initiate more accurate region growing procedures. Statistically based local thresholding is applied to calculate upper and lower threshold values which control the spatial extents of the final detected regions. The technique has been tested on full-disk solar images from the Meudon Observatory for the two months of April and July 2002 and compared with their manually generated synoptic maps. Figure 3 shows some active region detection results, Figure 3a shows a cleaned Meudon CaII K3 image which is the input to the procedure, Figure 3b shows the results of remapping into the polar coordinates, Figure 3c shows the results of the initial segmentation Figure 3d shows the detected regions after applying median and morphological processing and transformation back to Cartesian coordinates and finally Figure 3e shows the final results of applying the region growing procedure superimposed on the cleaned image. Figure 4a shows a close-up of a detected active region. Figure 4b shows the boundary of the detected active region, which is stored using a chain code (Benkhalil *et al.*, 2005).

A quantitative comparison was made between the results obtained using the present technique, those done manually at the Meudon Observatory (Mouradian, 1998) and those done by the National Oceanic and Atmospheric Administration Observatory (NOAA). In order to quantify the comparison, the FAR and the FRR were calculated for each day. Generally Meudon lists significantly more active regions than either us or NOAA. For most days a higher number of active regions were detected by us than by NOAA with an average FAR of 1.7 per day. The FRR

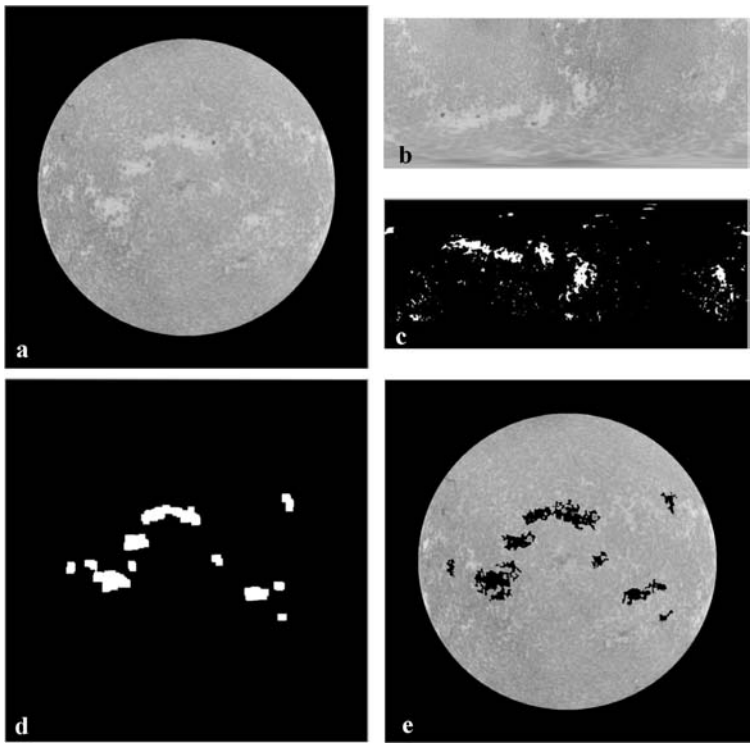

Figure 3. The segmentation procedure stages: (a) an original CaII K3 image; (b) the image after a transformation to polar coordinates; (c) after an initial thresholding; (d) after a transformation back to Cartesian coordinates, cleaning and morphological processing and (e) the final results of a region growing for the whole disk image (from Benkhalil *et al.*, 2005).

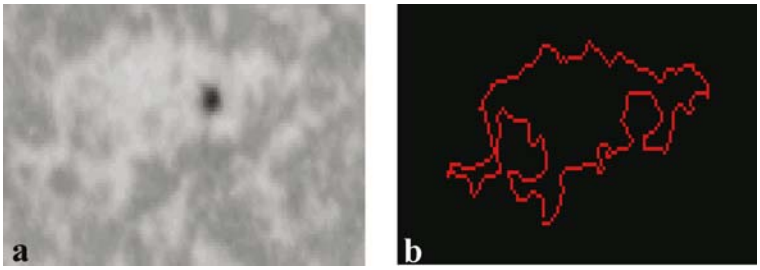

Figure 4. An active region boundary detection: (a) a close-up of the detected active region and (b) a boundary of the detected active region used for representation with a chain code (see for details Section 4 and Aboudarham and Zharkov, 2004).

of 0.2 was very low and there are only 5 days when we failed to detect a region detected by NOAA. In some cases we detect an active region while NOAA splits it into two regions. This affects the quantitative comparison.

In general, in April 2002 the accuracy of active region detection with the presented technique was 96% in comparison with the NOAA active regions but

only 55% in comparison with the Meudon active regions, or plages. A similar trend is repeated in July with the detection accuracy 97% comparing to the NOAA dataset and 40% to the Meudon one. The reason for such different results is due to the differences adopted for the definition of an active region by these two observatories. At Meudon all bright regions (plages) are detected, and these are defined as active regions, or plages, in the chromosphere that are brighter than the normal "quiet" Sun background. At NOAA a detected active region is defined as a bright area on the Sun with a large concentration of magnetic field, often containing sunspots if they are not decaying active regions with a weakening magnetic field. The number of active regions for Meudon can be increased by lowering the local threshold value but this will increase their differences from the NOAA results. In order to resolve the differences a discussion is required among the observers on the active region definitions.

In general, in the frame of each observatory definitions, the procedures developed by us for the automated detection of active regions, have achieved a satisfactory accuracy in the detection and segmentation of active regions using full disk Hα and CaII K3 solar images from the Meudon Observatory and full disk FeXII 195 Å solar images from SOHO. The structure of active regions at various levels of the solar atmosphere can provide a key to the understanding and reliable forecast of solar activity manifestations such as: solar flares, coronal mass ejections (CMEs), eruptive filaments etc. The parameters extracted from automatically detected active regions, such as their location, sizes, intensities (max, min and mean) are populated into the *active region feature table* of the SFC database discussed in Section 4.

3.3. FILAMENT DETECTION

Filaments are chromospheric features which are denser and cooler than their surroundings, thus appearing as dark features when seen against the Hα light of the disk. They can be automatically detected on Meudon Observatory Hα full-disk observations, using a hybrid region growing technique (Fuller and Aboudarham, 2004; Fuller, Aboudarham, and Bentley, 2005), providing that these images are previously cleaned (Zharkova *et al.*, 2003). Some other methods have already been proposed to detect filaments (Collin and Nesme-Ribes, 1992; Gao, Wang, and Zhou, 2002; Wagstaff *et al.*, 2003; Shih and Kowalski, 2003; Zharkova and Schetinin, 2003) using either advanced region based techniques or an artificial neural network. The method described here was designed to extract the most complete set of filaments from a given image.

Once the images are cleaned from possible dark lines across the disk (due to dust particles) and enhanced using a sharpening spatial filter (Fuller and Aboudarham, 2004; Fuller, Aboudarham, and Bentley, 2005), the seeds of filaments are investigated in order to initiate the region growing process. This is achieved by dividing the image into square windows where the mean and standard deviation of pixels are

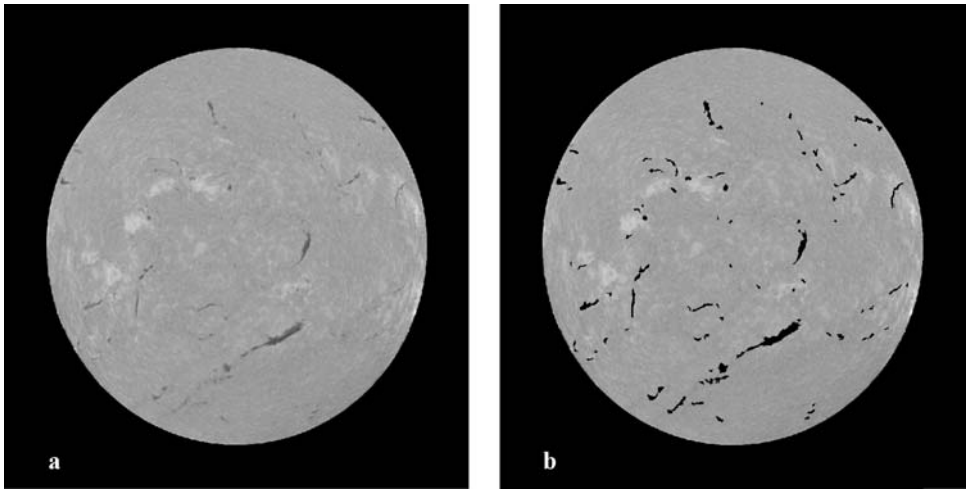

Figure 5. Filament regions detection in the Hα line full-disk image obtained at the Meudon Observatory on April 2, 2002: (a) The original image after cleaning, (b) the final detection results superimposed on the cleaned image

calculated in order to compute a local threshold. If a seed is larger than a limit size, it is considered for further processing. The next step is to grow the seeds according to the statistics of the local pixels. A bounding rectangle is defined from the location and size of the seed allowing us to compute the mean and standard deviation of the neighboring pixels. A higher threshold value is obtained from these values, which determines whether a neighboring pixel is appended to the seed or not. Figure 5 shows the filament detection results in the Hα line image.

Once the image is segmented we need to give a simpler representation of the shapes, in order to compute descriptors such as the length, center or curvature of the filament. Given the pruned skeleton of the region, using morphological operators (Fuller, Aboudarham, and Bentley, 2005), we reduce it to its centerline (see Figure 6). This representation could also be useful for the detection of filament barbs (Wagstaff *et al.*, 2003). It also permits one to compare the automated detection with those done manually at the Meudon Observatory.

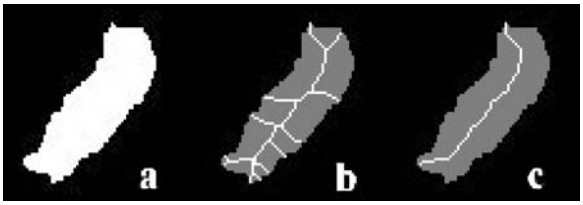

Figure 6. Filament skeleton: (a) The original shape, (b) the full skeleton tree and (c) the pruned skeleton.

For the month of April 2002 we missed 10.9% of total 1232 filaments manually recorded providing an accuracy of detection about 89%. The 'false negatives' are mostly associated with short or faint filaments. However, looking at each individual observation, we can confirm that none of the important filaments were missed, except those which are too close to the limb and are discarded by the detection process. The comparison results satisfactorily represent the major filaments on the synoptic maps and confirm that the method can effectively be used in the frame of the EGSO project in order to produce a reliable set of filament detections.

This detection is now complete for the dataset of daily Hα images captured in 1996 – 2004 at the Meudon Observatory. The parameters automatically extracted from the filaments, such as their location, skeleton length, intensities (max, min and mean) and others, are populated into the *filament feature table* of the Solar Feature Catalogue discussed in Section 4.

4. Searchable Database of Solar Features

Extracted parameters of the detected features (sunspots, active regions and filaments) were stored as ASCII files in the relevant format according to the Feature Parameter (FP) document (Aboudarham and Zharkov, 2004), which are used to populate the MySQL searchable database. The database was designed to include the parameters describing the pre-processing and feature-detection code that was used for the extraction of the feature parameters as well as observational and individual feature parameters themselves. The database is published on *http://www.cyber.brad.ac.uk/egso/SFC/SFC_form.html*. This allows one to search by time, location and size of a feature and can be downloaded in the ASCII or XML formats.

The detection process for each feature can be summarized as follows:

First the initial observation (a full disk image from the archive) is pre-processed using the automated cleaning technique (Zharkova *et al.*, 2003) described in Section 2. The cleaning code setup generally depends on the source of the observation, or chosen archive. Then the features of interest are detected using the feature recognition methods described in Section 3; these include sunspots active regions (plages) and filaments. For each type of feature a number of parameters described in FP (Aboudarham and Zharkov, 2004) are extracted. Each feature's boundaries are stored as a set of pixels in the pre-processed image being either a Bounding Rectangle Raster Scan for sunspots or a Chain Code for filaments and active regions (plages).

Hence, the database contains the following tables related to original observation (Figure 7):

Observation table:

- Observations, which includes the observational parameters as related to the original observation;

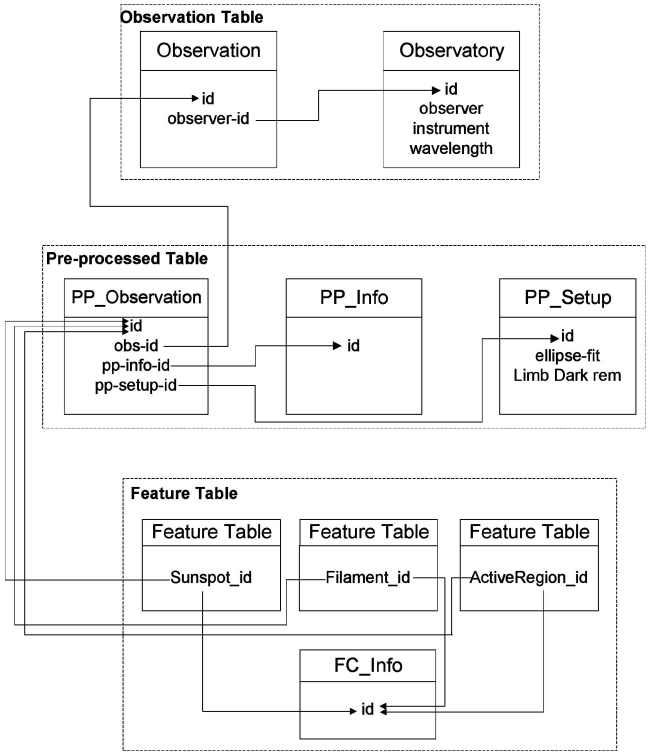

Figure 7. The SFC database structure containing the observation table, pre-processing table and feature tables for sunspots, active regions and filaments (see Section 4 for more details).

- Observatory, which contains parameters related to the Observatory/Instrument (linked to Observations).

The following tables are related to pre-processing stage:

Pre-processing table:
- Pre-Processing Info – contains information about pre-processing code version, where it was run, etc.
- Pre-Processing Setup – which describes pre-processing code settings and input parameters.
- Pre-Processing Output – which contains the parameters which have been extracted or amended in the pre-processing stage, such as (where applicable) quiet-Sun intensity, image size, resolution, solar disk radius,
- Ellipse fitting parameters.

And finally the tables related to the feature recognition itself:

Feature tables:

This table contains the individual feature parameters describing each detected feature: sunspots, faculae, filaments.

- Feature Recognition Code Info – provides the information describing the code used for the extraction of feature parameters.
- Feature parameters themselves – location, size, area, intensity ratios to the quiet sun intensities and many others, variable for different features (for details see Aboudarham and Zharkov, 2004).

The database structure is organized in such a way that each feature has an identification number related to a processed observation (one record in Observation Output), to pre-processing setting (one record in Pre-Processing Output) and to the Feature Information itself (one record in Feature output). Each original observation (image) is associated with one entry from the Observation table including an observatory, observation time, wavelength, cadence etc. Each pre-processed image is related to its original observation with the observation ID that also provides an additional entry from the Pre-Processing Setup where the Pre-Processing information is recorded. This can be used for the feature restoration onto other images not used in the automated recognition process.

Then for each observation the features are detected and their identification numbers for a given date are assigned. Since there are 3 types of features extracted on every date, so the different identification numbers are assigned to sunspots, active regions (plages) and filaments. Each of these three IDs has entries to the pre-processing and observation tables as shown in the diagram in Figure 7. Hence, this allows one to uniquely identify every feature appearance in the original image and to relate it to the original observation time.

5. Conclusions

In the present paper the automated procedures for detection of the solar features: sunspots, active regions and filaments in full-disk solar images are briefly described. The original images are automatically standardized by shape and intensity in which the feature detection techniques are applied with local intensity thresholding. For compact features, like sunspots gradient, edge detection methods are used while for extended features of plages or filaments region growing method was used combined with suitable image filtering and morphological operations. The parameters extracted from the detected features (size, location, area, intensities, borders, etc.) are populated into the relational database of the Solar Feature Catalogues for sunspots (WL images, SOHO/MDI), active regions (CaII K3 images, MO) and filaments (Hα images, MO) obtained with reasonable accuracy for the period of May 1996–December 2004. The accuracy can be further increased by agreed definitions of the features under investigation based on their digital image properties and classification

of related physical properties that requires a discussion between the experienced observers from the observatories providing such the datasets.

The current database is integrated into the EGSO grid as a special provider metadata as described in the Section 4. The EGSO users who are interested in a particular feature observed at a given time and coordinates, will use the Solar Event Catalogue (another metadata created from the existing event catalogues) to define the precise time and location and then with these data they will access the Solar Feature catalogue, extract the features required and over-plot them onto any image. The possible tasks are listed in the 'Use cases' document on the BU web site *http://www.cyber.brad.ac.uk/egso/Doc/Doc.html*.

Another set of tasks to be investigated with the SFCs is related to feature tracking during its pass across the solar disk and to various statistical analysis of the features in a given period of time, in any given locations and their associations with the other features. The SFCs with the information on each feature stored in the database can be used for the single feature classification and their joint utilization as the solar activity flags. This can help to identify the classifiers responsible for the solar activity and to produce a short-term and long-term solar activity forecast based on the SFCs.

Acknowledgements

The authors would like to acknowledge the financial support of the European Commission as a part of the EGSO Project within the IST Framework 5, grant IST-2001-32409.

References

Aboudarham, J. and Zharkov, S.: 2004, *http://www.cyber.brad.ac.uk/egso/Doc/Doc.html*, Features Parameters Description and Organization, EGSO-WP5-IR3-2.3, p. 36.

Baxes, G.: 1994, *Digital Image Processing: Principles and Applications*, Wiley, p. 657

Benkhalil, A. K., Zharkova, V., Ipson, S., and Zharkov, S.: 2003, *Proc. AISB'03 Symp. Biologically-Inspired Machine Vision, Theory and Application*, University of Wales, Aberystwyth, 7–11 April 2003, p. 66.

Benkhalil, A. K., Zharkova, V., Ipson, S., and Zharkov, S.: 2004, *Proc. 8th Int. Conf. Knowledge-Based Intelligent Information and Engineering Systems* (*KES2004*), Springer *Lecture Notes in Computer Science*, LNAI 3215, **3**, 460.

Benkhalil, A. K., Zharkova, V., Ipson, S., and Zharkov, S.: 2005, *J. Comp. Apps* (*ISCA*), ID #3303AP, in press.

Bentley, R. D. and EGSO Consortium: 2002, *Proc. 10th Eur. Solar Phys. Meeting*, 9–14 September 2002, Prague, Czech Republic, A.Wilson (ed.), ESA SP-506, Vol. 2, ISBN 92-9092-816-6, p. 923.

Brandt, P. N., Schmidt, W., and Steinegger, M.: 1990, *Solar Phys.* **129**, 191.

Canny, J.: 1986, *IEEE Trans. Pattern Anal.* **6**, 679.

Casasent, D.: 1992, *Proc. SPIE Conf. Intelligent Robots Comput. Vision XI*, **1825**, 2.

Chapman, G. A. and Groisman, G.: 1984, *Solar Phys.* **91**, 45.

Chapman, G. A., Cookson, A. M., and Dobias, J. J.: 1994, *Astrophys. J.* **432**, 403.

Collin, B. and Nesme-Ribes, E.: 1992, *Proc. ESA Workshop Solar Phys. Astrophys. Interferometric Resolu.*, Paris, 17–19 February 1992, p.145.

Fuller, N. and Aboudarham, J.: 2004, *Proc. 8th Int. Conf. Knowledge-Based Intelligent Information and Engineering Systems* (*KES2004*), Springer *Lecture Notes in Computer Science*, LNAI 3215, Vol. 3, p. 453.

Fuller, N., Aboudarham, J., and Bentley, B.: 2005, *Solar Phys.* (in press).

Gao, J., Wang, H., and Zhou, M.: 2002, *Solar Phys.* **205**, 93.

Györi, L.: 1998, *Solar Phys.* **180**, 109.

Hill, M., Castelli, V., Chung-Sheng, L., Yuan-Chi, C., Bergman, L., Smith, J. R., and Thompson, B.: 2001, *Int. Conf. Image Proc.*, Thessaloniki, Greece, 7–10 October 2001, **1**, 834.

Jackway, P., 1996, *IEEE Trans. Image Proc.* **5**, 913.

Mouradian, Z.: 1998, *Synoptic Solar Phys. ASP Conf. Series* **140**, 181.

Preminger, D. G., Walton, S. R., and Chapman, G. A.: 2001, *Solar Phys.* **202**, 53

Shih, F. Y. and Kowalski, A. J.: 2003, *Solar Phys.* **218**, 99.

Steinegger, M. and Brandt, P. N.:1998, *Solar Phys.* **177**, 287.

Steinegger, M., Bonet, J. A., Vazquez, M.: 1997, *Solar Phys.* **171**, 303.

Steinegger, M., Vazquez, M., Bonet, J. A., and Brandt, P. N.: 1996, *Astrophys. J.* **461**, 478.

Steinegger, M., Brandt, P. N., Pap, J., and Schmidt, W.: 1990, *Astrophys. Space Sci.* **170**, 127.

Turmon, M., Pap, J. M., Mukhtar, S.: 2002, *Astrophys. J.* **568**, 396.

Veronig, A., Steinegger, M., Otruba, W., Hanslmeier, A., Messerotti, M., and Temmer, M.: 2001, *HOBUD7*, **24**(1), 195.

Wagstaff, K., Rust, D. M., Labonte, B. J., and Bernasconi, P. N.: 2003, Solar Image Recognition Workshop, Brussels, 23–24 October 2003.

Worden, R., White, O. R., and Woods, T. N., 1996, *Solar Phys.* **177**, 255.

Zharkov, S. I. and Zharkova, V. V.: 2005, *Adv. Space Res.*, submitted.

Zharkov, S. I., Zharkova, V. V., and Ipson, S. S.: 2005, *Solar Phys.* (this issue).

Zharkov, S. I., Zharkova, V. V., Ipson, S. S., and Benkhalil, A. K.: 2003, *Proc. AISB'03 Symp. Biologically-Inspired Machine Vision, Theory and Application*, University of Wales, Aberystwyth, 7–11th April 2003, p. 74.

Zharkov, S. I., Zharkova, V. V., Ipson, S. S., and Benkhalil, A. K.: 2004, *Proc. 8th Int. Conf. Knowledge-Based Intelligent Information and Engineering Systems* (*KES2004*), Springer *Lecture Notes in Computer Science*, LNAI 3215, Vol. 3, p. 446.

Zharkova, V. V. and Schetinin, V.: 2003, *Proc. 8th Int. Conf. Knowledge-Based Intelligent Information and Engineering Systems* (*KES2003*), Part I, ISBN 3-540-40804-5, p. 148.

Zharkova, V. V., Ipson, S. S., Zharkov, S. I., Benkhalil, A. K., Aboudarham, J., Bentley, R. D.: 2003, *Solar Phys.* **214**(1), 89.

Zharkova, V. V., Ipson, S. S., Zharkov, S. I., and Benkhalil, A. K.: 2005, *J. Artificial Intelligence Rev.*, Springer Science and Business Media B.V., 58 pp, in press.